International Journal of Engineering Research and Development
e-ISSN: 2278-067X, p-ISSN: 2278-800X, www.ijerd.com
Volume 12, Issue 3 (March 2016), PP.22-38

Numerical and Experimental Analysis of a Solar Air Heater for Improved Performance

Sukrut Surendra Prabhu
Department of Mechanical and Manufacturing Engineering, Manipal Institute of Technology, Manipal, India

Abstract: -A literature review carried out by the authors reveals that a CFD analysis has not been the focus of attention to evaluate the efficacy of obstacles for improving the thermal performance of solar air heaters. A three dimensional CFD analysis is carried out in the present work to augment the performance of solar air heater. A circular obstacle in the flow path is used in this study to improve the flow turbulence and thereby enhance the convective heat transfer to air. The numerical results are validated with experimental results for model with and without obstacle. The numerical results show that obstacles are useful in enhancing the heat transfer rates. However with introduction of the obstacle there is increase in the pressure drop as compared to plane model. This increase in pressure drop has been reduced by introduction of fillet in flow path.

Keywords:- Configuration, Nusselt number, Pressure drop, Temperature co-efficient, Numerical, Experimental.

I. INTRODUCTION

Solar air heaters are devices that utilize solar radiation for a variety of purposes to obtain clean energy for a wide usage. These devices are simple and can be constructed inexpensively. The solar air heater device intercepts solar radiation, converts this radiation to the heat in air and delivers the air for use. Mainly, solar air heaters consist of a transparent cover, an absorber plate and insulation material. The air flow enters through the channel that is formed by the absorber plate and the transparent cover. Solar radiation absorbed by the absorber plate. The absorbed heat transferred to the air as it flows along the channel increases its temperature. . The use of a blower is optional for the air supply .This heated air can be used in several applications such as drying agricultural products, space heating and air conditioning, water heating and industrial process heating. There are many advantages of solar air heater systems. Firstly, they are simple to maintain and design. After the set-up cost, a solar air heater system has no fuel expenditure. There is less leakage and corrosion when compared to the systems that use liquid. It is also an eco-friendly system which has zero greenhouse gas emissions.
Any improvement in the performance of solar heater will contribute significantly since air heaters are widely used for commercial and industrial applications.

The primary disadvantage of these systems is the low heat transfer coefficient compared to systems that use liquid as the working fluid. This is the result of low heat transfer coefficient between the absorber plate and the air. Low heat transfer coefficients lead to low thermal efficiency of solar air heaters. For many years researchers have studied the enhancement of heat transfer coefficients of solar air heaters. To increase the efficiency of such a system, various configurations and designs have been proposed. The efficiency of solar air heaters can be affected by various parameters such as collector length, number of channels, depth of channels, type of absorber plate, number and material of glass covers, air inlet temperature and air velocity.

II. OBJECTIVE AND METHODOLOGY

OBJECTIVE: To design a solar air heater which develops a better convective heat transfer compared to other conventional air heaters**.**
METHODOLOGY: 1.To study the existing air heaters those are in commercial use. 2. To design an air heater as per the ASTRA standards. 3. To carry out a CFD analysis of the designed collector and compare it with conventional collector. 4. To validate the CFD results with experimental results by fabricating the designed collector. 5. Analyse the experimental and CFD results and plot the performance graphs.

III. NUMERICAL ANALYSIS

For the numerical analysis, 5 different configurations of air heater were adopted and CFD analysis was carried out using the FLUENT 14.5. The modelling and meshing was carried out using GAMBIT software. The first configuration which is base model consists of an air heater with a rectangular cross section of 250mm width and 30mm height and 1200mm length as shown in the figure 1. The absorber plate is 0.5mm in thickness and is made of copper.

A. Numerical Configurations

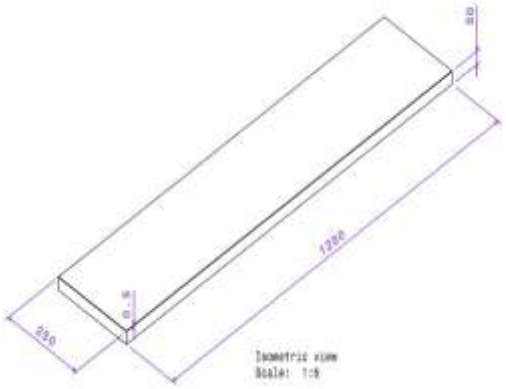

Fig: 1 Configuration 1

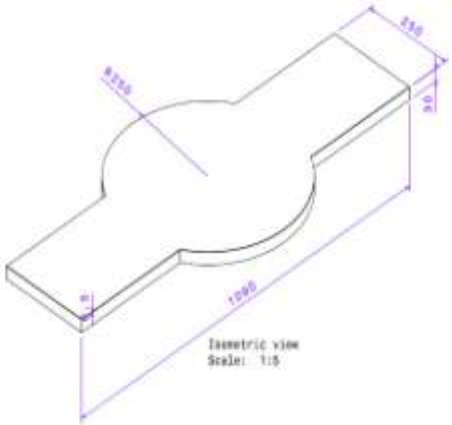

Fig: 2 Configuration 2

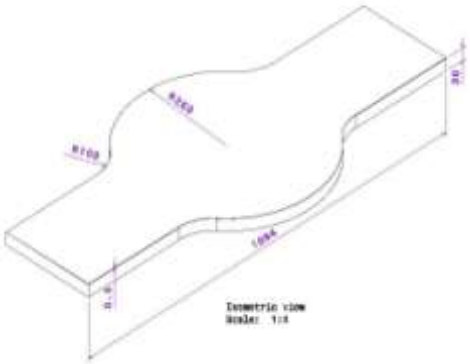

Fig: 3 Configuration 3

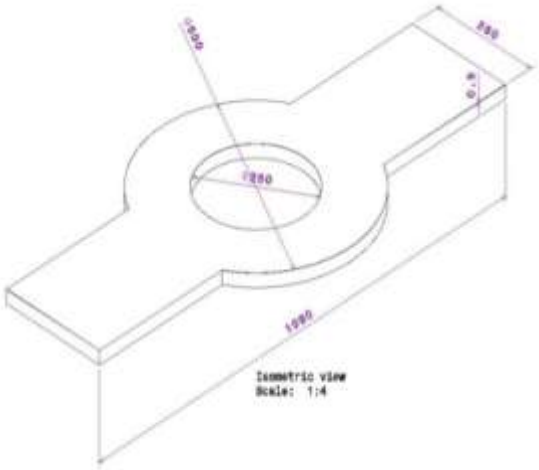

Fig: 4 Configuration 4

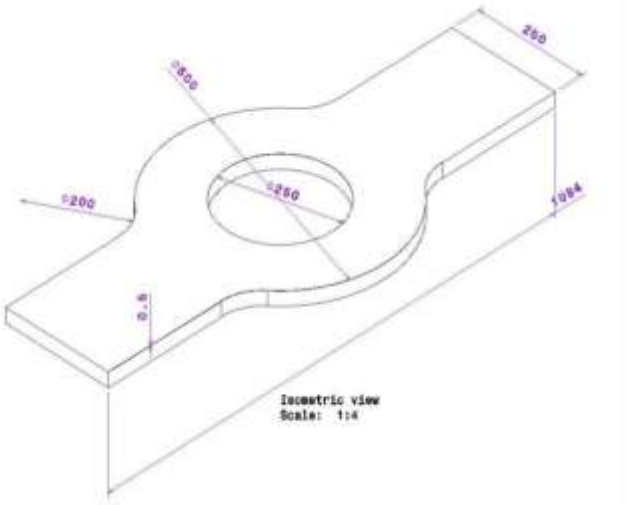

Fig: 5 Configuration 5

The second configuration has an obstacle of 250mm diameter introduced at the middle of the duct and the obstacle is made of copper as shown in the figure 2.The third configuration is similar in design to configuration 2 but a fillet is introduced in the model so as to ensure smooth air flow as shown in figure 3.The

fourth configuration in figure 4 has an obstacle of 250 mm diameter introduced at the middle of the duct with no absorber plate covering it and no fillet given. The fifth configuration shown in figure 5 is similar in design to configuration 4 but the only difference is that there are fillets given in this configuration.

The following assumptions are made in the analysis.
1. Air is a continuous medium and compressible.
2. The flow is steady and possesses turbulent flow characteristics, as the air moves over the roughened surface with the presence of obstacle.
3. The thermo-physical properties of the absorber plate are constant with respect to the operating temperature.
4. The bottom surface and the side surfaces of the air domain is assumed to be adiabatic.
5. A constant value of heat flux is assumed on the absorber plate to simulate solar insulation.

B. Numerical Formulation

Numerical simulation is carried out with steady state implicit pressure based solver using the Fluent code 14.5 The governing partial differential equations, for mass and momentum are solved for the steady state flows. The pressure-velocity coupling is carried out using the SIMPLE algorithm of Patankar (1980). Discretization is done using the second order upwind scheme.
Mean Flow Equations:
All the equations are presented in Cartesian tensor notation as shown in figure 6.

Continuity:

$$\frac{\partial}{\partial x_i}(\rho U_i) = 0 \qquad (1)$$

Momentum equation:

$$\frac{\partial}{\partial x_j}(\rho U_i U_j) = \frac{\partial P}{\partial x_i} + \frac{\partial}{\partial x_j}\left[\mu\left(\frac{\partial U_i}{\partial x_j} + \frac{\partial U_j}{\partial x_i}\right) - \rho\overline{u_i u_j}\right] \qquad (2)$$

Energy equation:

$$\frac{\partial}{\partial x_j}(\rho U_i T) = \frac{\partial}{\partial x_j}\left[\frac{\mu}{\mathrm{Pr}}\frac{\partial T}{\partial x_j} - \rho\overline{u_i t}\right] \qquad (3)$$

Fig: 6 Mean Flow Equations

For modelling and meshing as shown in figure 7, GAMBIT was used. In which firstly a face was created for the models having Quad elements of Pave type with interval size of 3.This face was extruded further by 0.5 mm along the edge which was meshed with successive ratio 1 and interval count 4 to create the absorber plate. Now, to create the air medium the face mesh was extruded along 30 mm mesh with successive ratio 1.05 and interval count 36.The mesh density was given more for the air mesh towards the absorber plate side to accommodate for boundary layer separation .
Based on this the number of elements formed in different configurations is summarized in table noI.

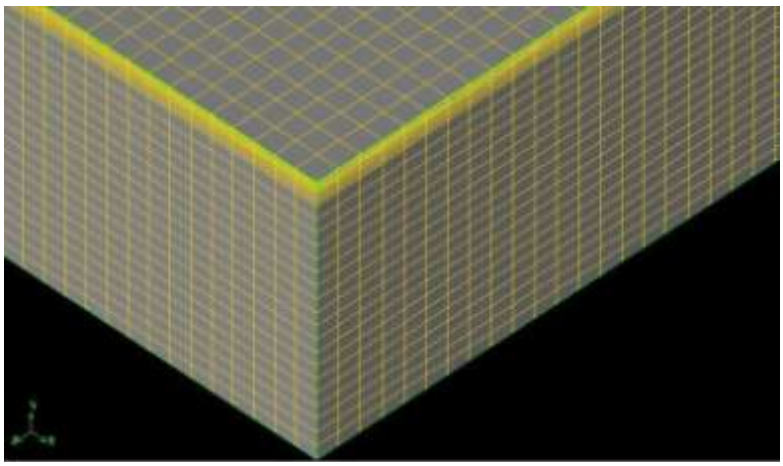

Fig: 7Meshed model

Table I:Number of elements formed in different configurations

Sl No.	Configuration	Number of Elements
1	Configuration 1	1200837
2	Configuration 2	1396041
3	Configuration 3	1389509
4	Configuration 4	1368536
5	Configuration 5	1352504

In case of air their properties such as density, specific heat thermal conductivity and viscosity were expressed in terms of function of absolute temperature as mentioned below:
Density = (3.9147) - (0.016082 X T) + (2.9013X10-5XT2)-(1.9407 X 10-8X T3)
Specific Heat= 1006.43
Thermal Conductivity = (1.5215 X 10-6) + (9.7459 X10-5 X T)-(3.3322X10-8XT2)
Viscosity = (1.6157 X 10-6) + (6.523 X10-8 X T)-(3.0297X10-11XT2)
The properties used for copper are-
Density=8978 kg/m3
Specific heat=381
Thermal Conductivity=387.6 w/m-k

The following values were chosen after going through several experimental data
Heat Flux =900 W/m2
Inlet Air velocity =5 m/s
Turbulent Intensity (%) = 5
Hydraulic Diameter (m) = (4 x Area/Perimeter) = [4 x 250 x 30 / {2 x (250+30)}] =0.05357----(1)
Convergence was affected when all the residuals in the computational domain fell below the mentioned values as shown in table II.

Table I:Residual values at convergence

Continuity	1e-05
x velocity	1e-05
y velocity	1e-05
z velocity	1e-05
Energy	1e-06
K	0.001
Epsilon	0.001

The performance parameters used for comparing the various configurations were:
1. Temperature coefficient = (To-Ti/Ti)
2. Nusselt number
3. Pressure drop across air heater
4. Absorber plate temperature coefficient = (T-Ti /Ti)

Where Ti is inlet air temperature and To is the outlet air temperature.

C. Analysis Steps

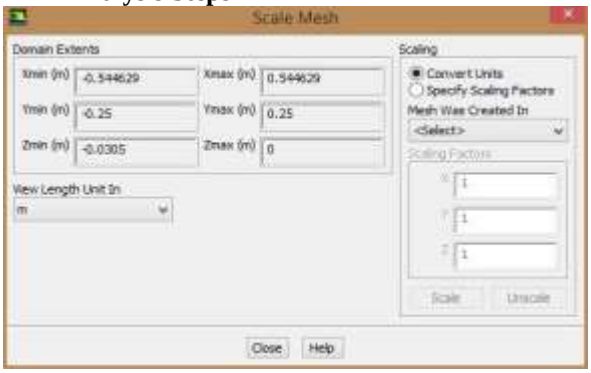

Fig: 8 Scaling

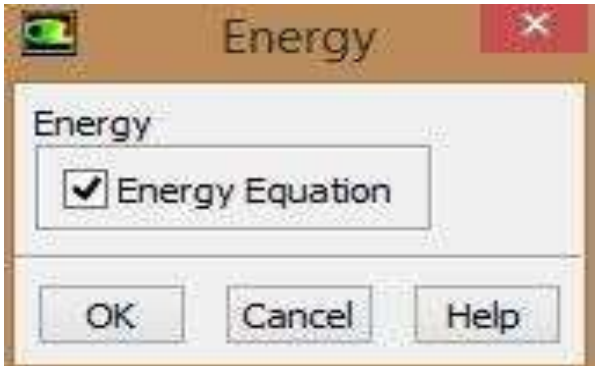

Fig: 9 Energy equation

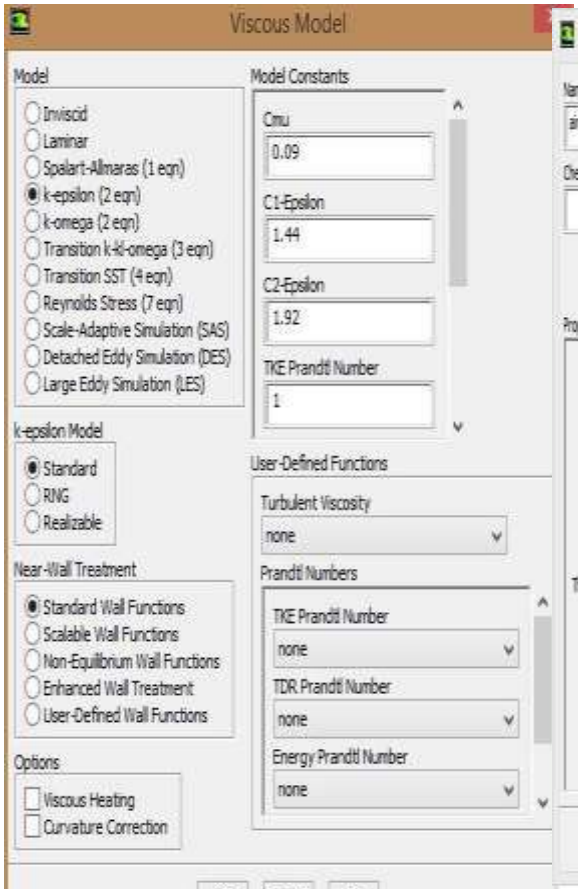

Fig: 10 Viscous model

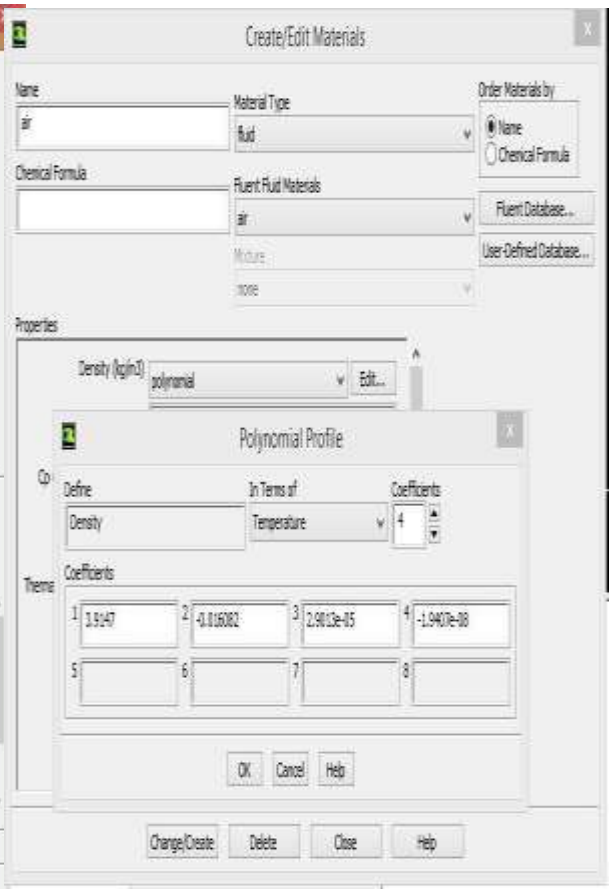

Fig: 11 Air density polynomial function

The figure 8 shows the scaling factor used for conversion of dimensions from mm to m. The figure 9 shows the selection of energy equation. The figure 10 shows the selection of viscous model being used.The next step in the process was to define the thermal and physical properties of air. Since properties of air like thermal conductivity, density and viscosity changes with change in temperature, polynomial function is defined with respect to temperature. This is shown in figures 11, 12, 13.While the figure 14 shows the input properties of copper material being used.

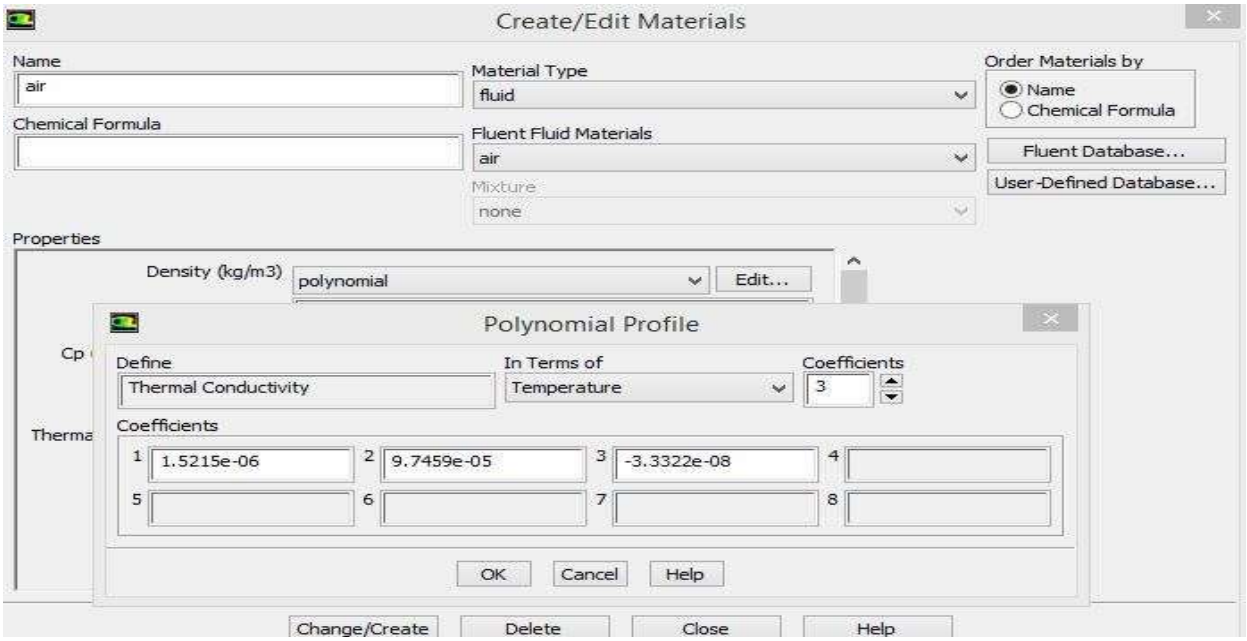

Fig: 12 Air thermal conductivity polynomial function

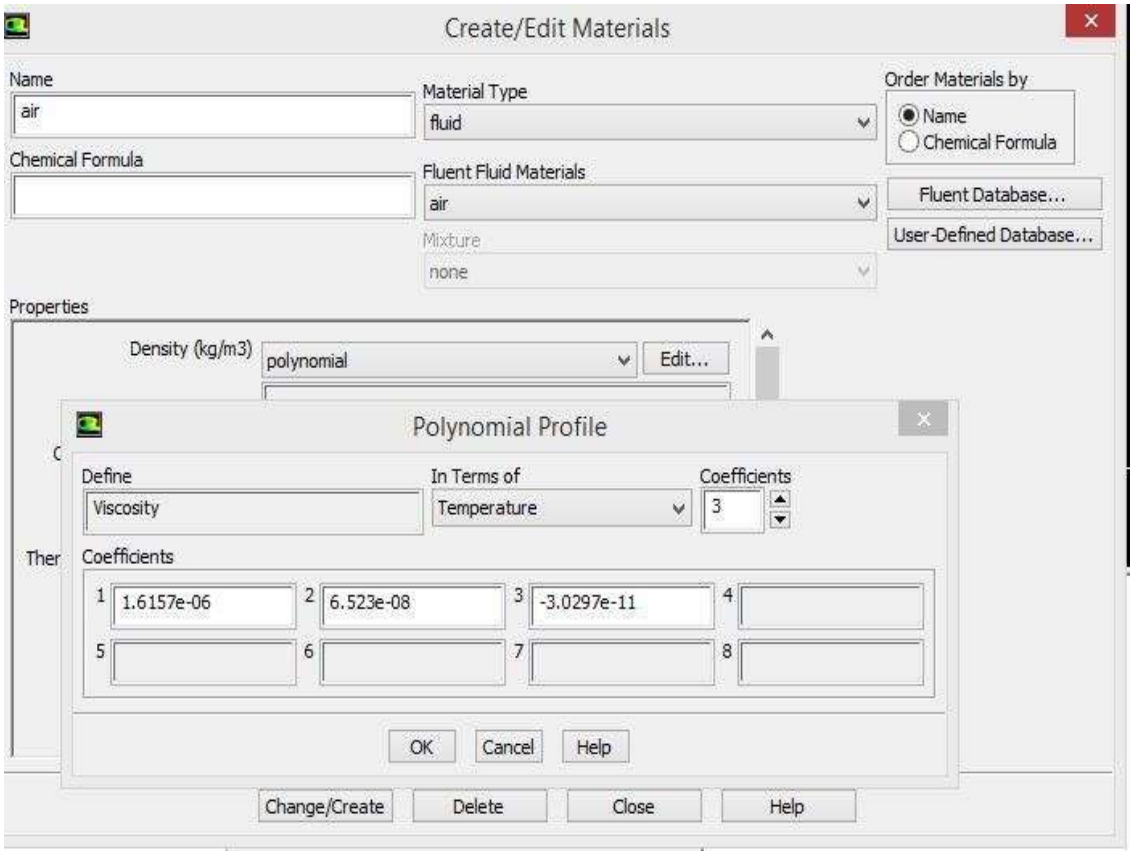

Fig: 13 Air viscosity polynomial function

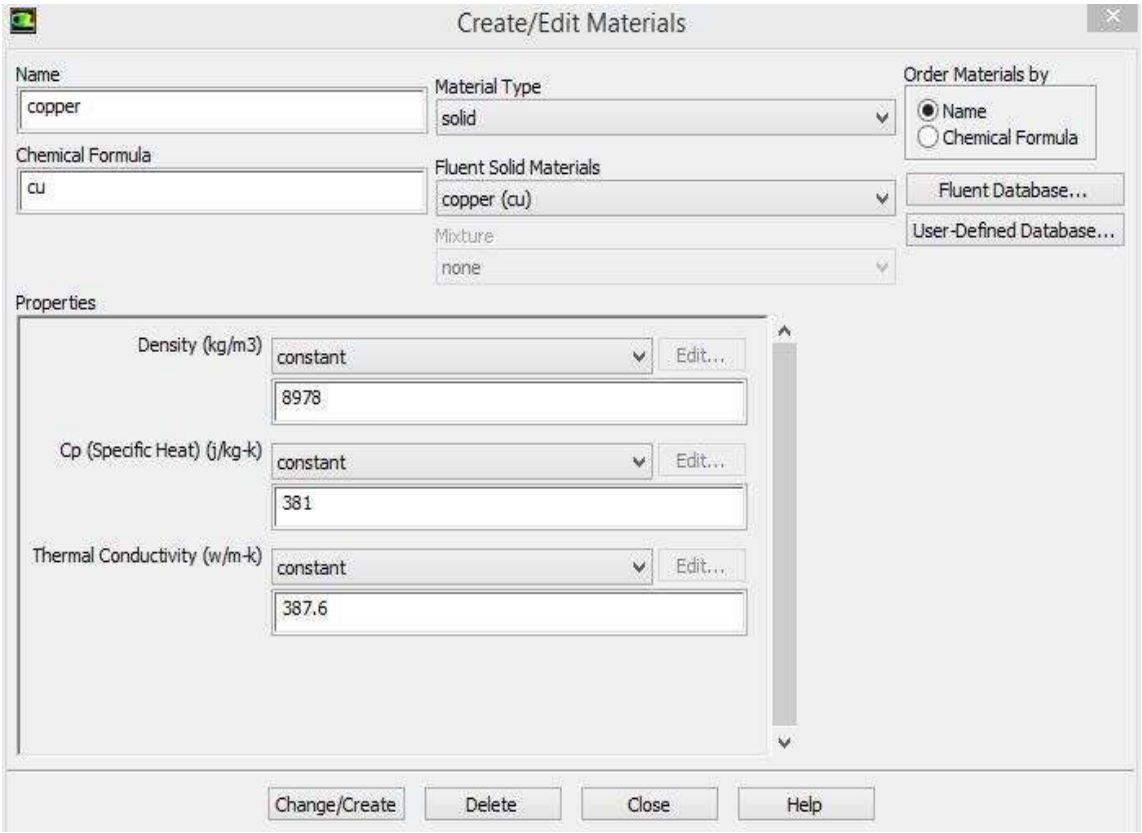

Fig: 14 Properties of copper

Next step is to define cell zone conditions of absorber plate, air, copper obstacle based on the boundary conditions.

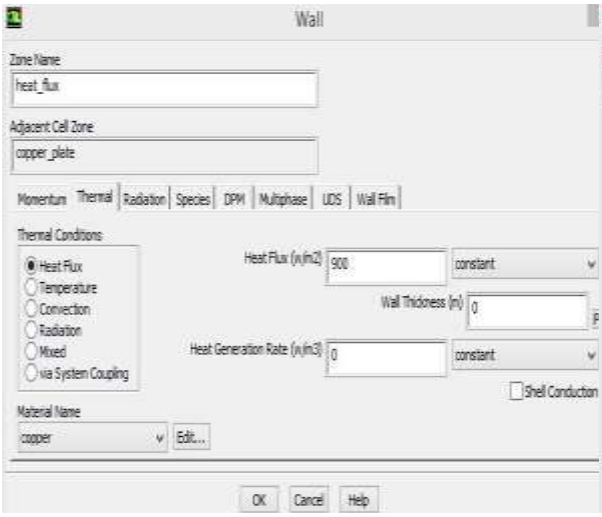

Fig: 15 Absorber plate cell zone conditions

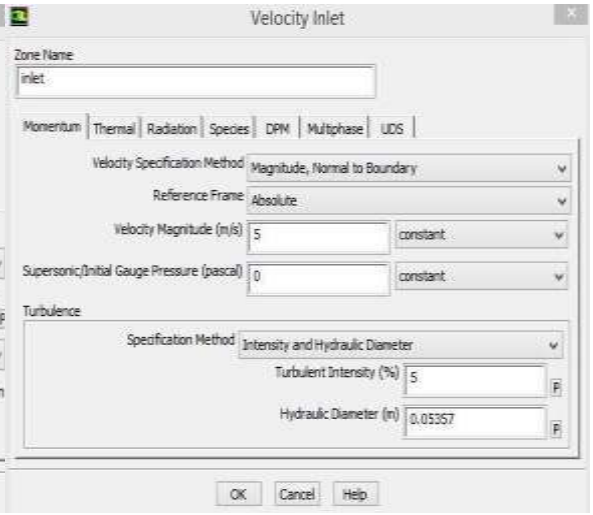

Fig: 16 Inlet momentum conditions

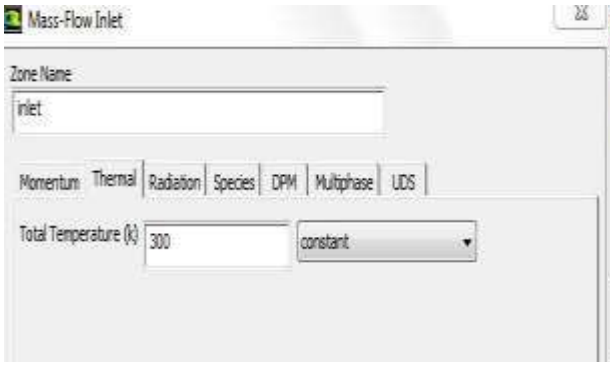

Fig: 17 Inlet thermal conditions

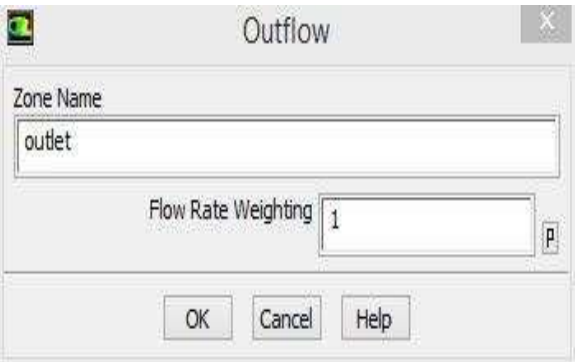

Fig: 18 Outlet

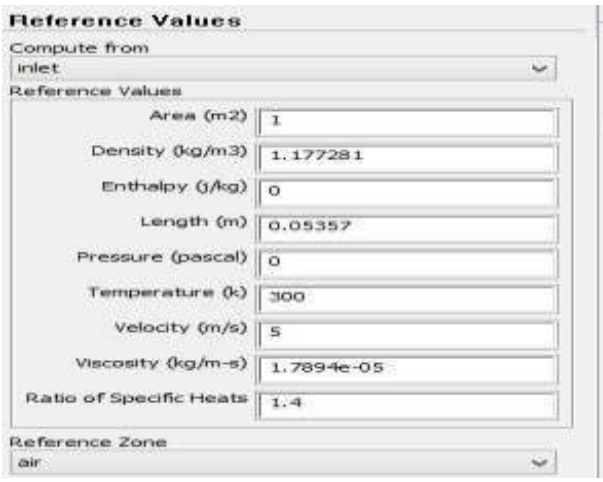

Fig: 19 Reference values

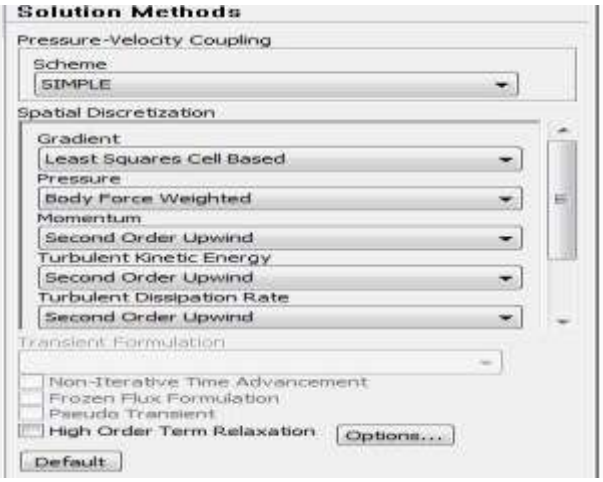

Fig: 20 Solution methods

As shown in figure 15, cell zone condition of Absorber Plate is defined with constant Heat Flux of 900w/m2.Inlet momentum conditions are shown in figure 16 which includes the input of hydraulic diameter, turbulent intensity, mass flow rate, direct specification method, etc. The temperature at inlet (300 K) is given by figure 17. Outlet is defined as type Outflow as shown in figure 18.The next step is to define the reference values. Computation starts from inlet. The length is taken as the hydraulic diameter whose calculation has been explained before in (1).Figure 20 shows the solution methods employed, SIMPLE scheme is adopted. Figure 21 shows the creation of one of the surface monitors. Here, five different surface monitors are made. They are Temperature at outlet, Pressure at Inlet, Pressure at Outlet, Nusselt Number at absorber plate, Absorber Plate Temperature.Figure 22 shows that we initialize using hybrid initialisation method and then calculation is started for 20000 iterations.

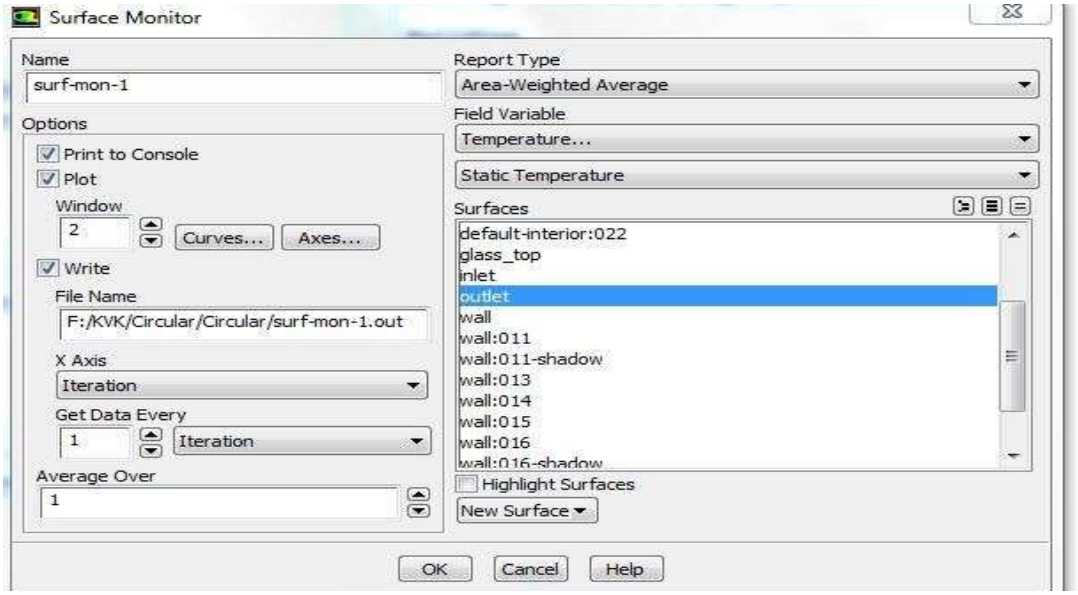

Fig: 21 Surface monitor

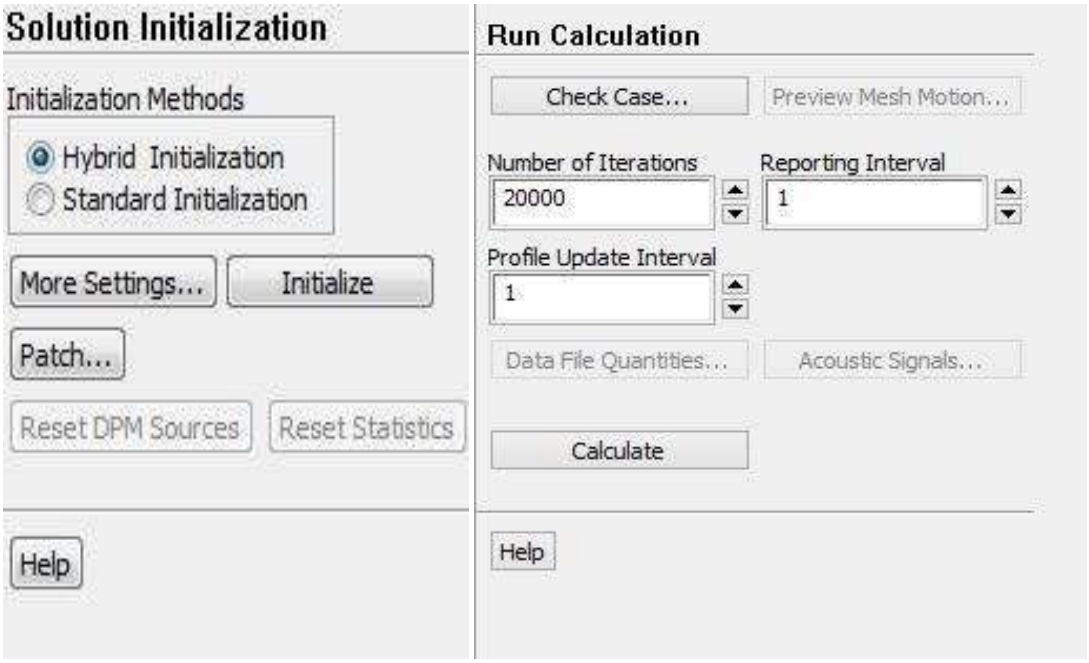

Fig: 22 Solution initialization and calculation

IV. EXPERIMENTAL VALIDATION OF NUMERICAL RESULTS

A. EQUIPMENTS USED

The materials used are plywood, copperplate, thermocouples etc. The air heating duct is fabricated using 1 inch thick plywood material and is 1.2 m long, 0.3 m wide and 30 mm in height. The upper surface is made up of a 0.5 mm thick copper plate which is the absorber plate exposed to solar radiation; data logger; thermocouples; thermal gun are used to measure temperatures at various points; M-Seal; nails and screws were used as additional components for joining. The various parts of experimental setup are as follows can be seen in figure 23 Entry duct, Model, Exit Duct.

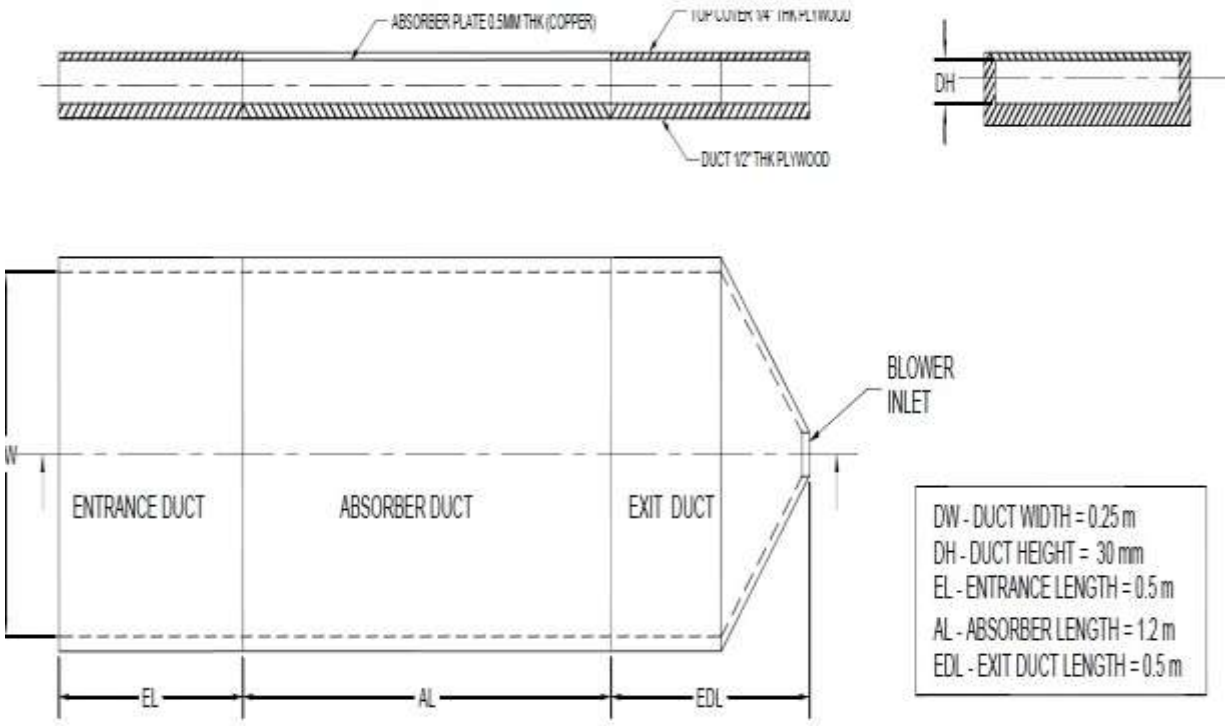

Fig: 23 Experimental Setup

B. EXPERIMENTAL PROCEDURE

The various devices used in the experimental setup as shown in figure 24 included thermal gun, solar radiation recorder, anemometer , data logger, RTD sensor, air blower, solar panel, pyranometer sensor, temperature sensor along with the two fabricated configurations.

Fig: 24 Experimental setup

The experimental validation was done with the help of two models i.e. configuration 1 and configuration 2.After the initial model fabrication was done with plywood, the absorber plate was painted black for it to absorb maximum radiation and attached on the top of the fabricated model by screwing . Three holes were drilled 20mm from exit duct along the axial direction and the RTD sensors were mounted equidistant and sealed using thin electrical tape. After this the blower was attached to the exit duct and sealed with duct tape to ensure there is no leakage of air. The entire model was tested to check whether there was any leakage.

The experiment was carried out as follows-
Both the configurations were kept side by side on the table as shown in figure under direct sunlight.
The models were kept in such a way that the length was in N-S direction.
The wires of the RTD sensors were connected to the Data logger.
The solar panel along with the solar radiation recorder was kept near the setup and then connected to the pyranometer sensor.
This pyranometer sensor was then attached on the table near the configurations.
Then the blowers were connected to the switch board along with solar radiation recorder to start off with the experimentation.
Both the blower speed were adjusted so that anemometer showed almost the same wind velocity at the inlet of the configuration and readings were taken at three different positions : right ,middle and left and average wind speed was noted
The heat flux intensity was noted at various intervals of time via the solar radiation recorder as it was varying throughout the experiment.
The RTD sensor attached to the data logger showed the air temperature just at the exit of the configuration flowing inside.
The inlet temperature was recorded with the thermometer.
The thermal gun was used to measure the absorber plate temperature at various points marked on the plate.
The readings were noted and compared to the numerical results.

C. EXPERIMENTAL RESULTS

Experimental readings are shown in the figures below for configuration 1 and configuration 2. Nine readings were taken to incorporate for variations in surrounding conditions and the average of all readings were taken into consideration and some of them are shown in figures 24, 25, 26 and 27.

1. Configuration 1

Inlet	Outlet
50.4	56.7
49	56.2
49.3	56
46.8	55.3

Average Velocity	2.566667
Heat Flux	800
Inlet Air Temperature	35
Outlet Air Temperaure	40.73333
Temperature Difference	5.733333

Fig: 24 Reading 1

50.3	58.4
47	57.1
49	56.5
50.2	56.8

Average Velocity	2.65
Heat Flux	792.5
Inlet Air Temperature	37
Outlet Air Temperaure	43.83333
Temperature Difference	6.833333

Fig: 25 Reading 2

2. Configuration 2

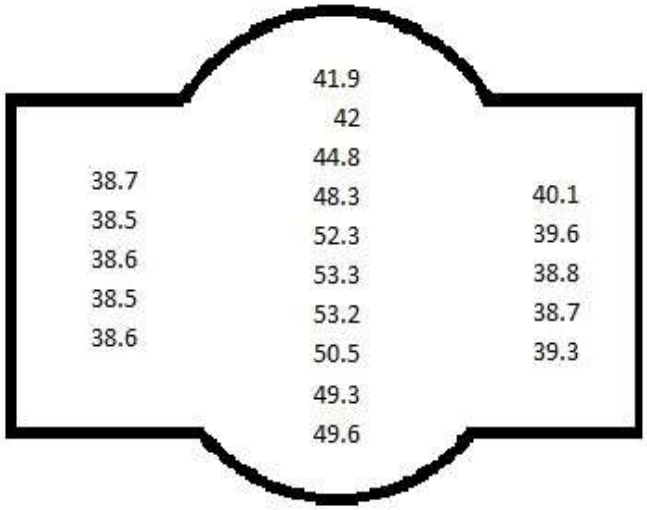

Average Velocity	2.7
Heat Flux	716.6667
Inlet Air Temperature	35
Outlet Air Temperaure	41.95
Temperature Difference	6.95

Fig: 26 Reading 1

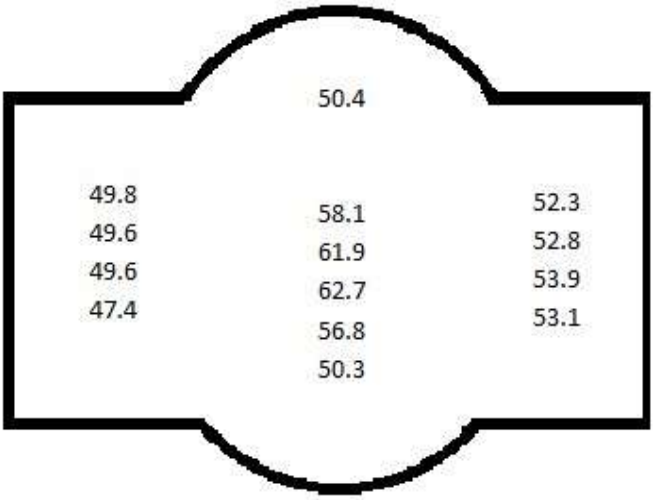

Average Velocity	2.466667
Heat Flux	825
Inlet Air Temperature	36
Outlet Air Temperaure	43.9
Temperature Difference	7.9

Fig: 27 Reading 2

V. RESULTS AND DISCUSSION

A. SIMULATION RESULTS

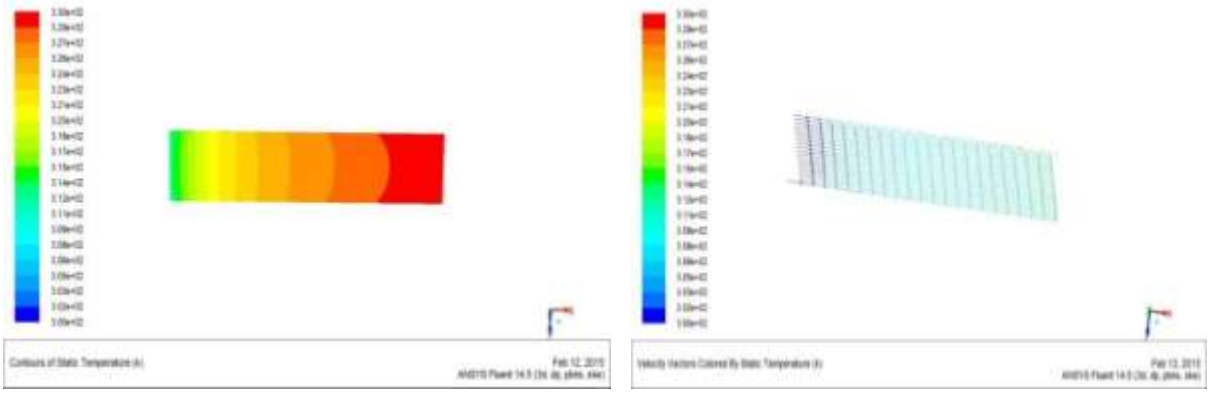

For Configuration 1 the results obtained after simulation for the basic model are as shown in figure 28The following plots were obtained- Absorber plate temperature, velocity vector, absolute temperature and static pressure.

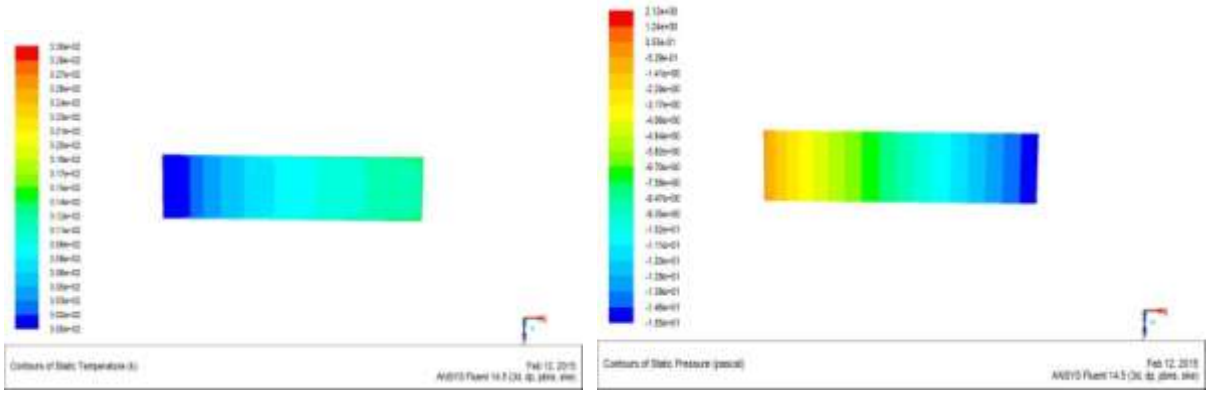

Fig: 28 Configuration 1 contour plots

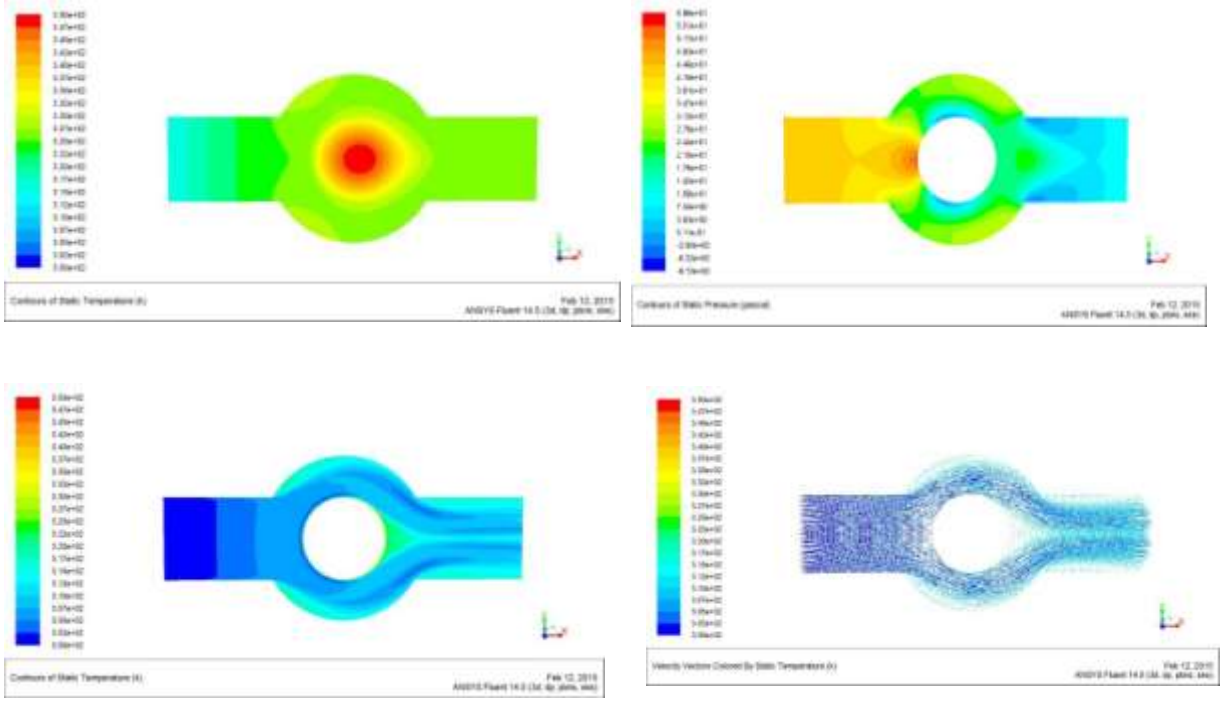

Fig: 29 Configuration 2 contour plots

For configuration 2 an obstacle is introduced in the basic configuration, although there is temperature and Nusselt number increase in this configuration which is favourable but the pressure drop is more which is unfavourable so further modifications need to be made. The results are as shown in figure 29 for configuration 2.

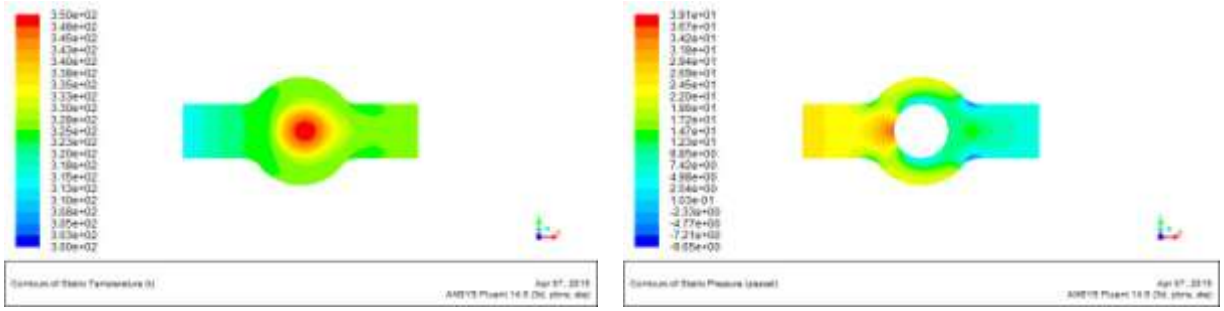

For configuration 3 a fillet is introduced in the 2nd configuration which has caused the pressure drop to decrease as compared to the 2nd configuration .The temperature and Nusselt number get slightly reduced as compared to the 2nd configuration. The results obtained are as shown in figure 30 for configuration 3.

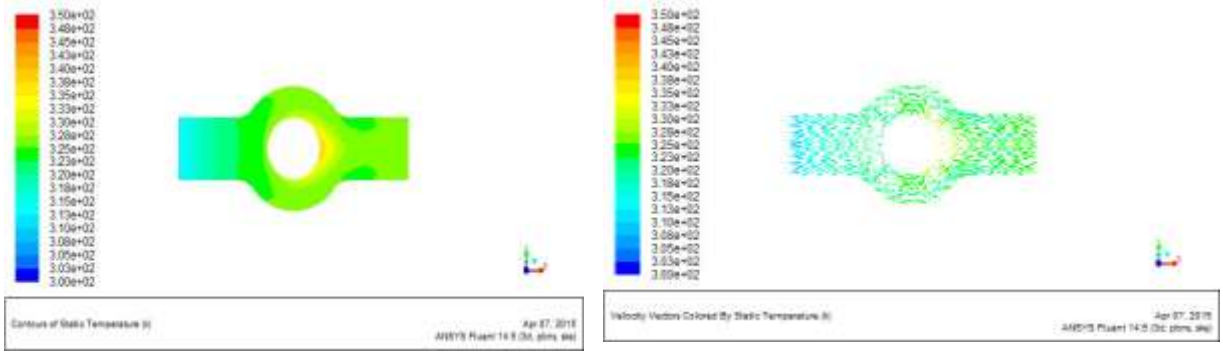

Fig: 30 Configuration 3 contour plots

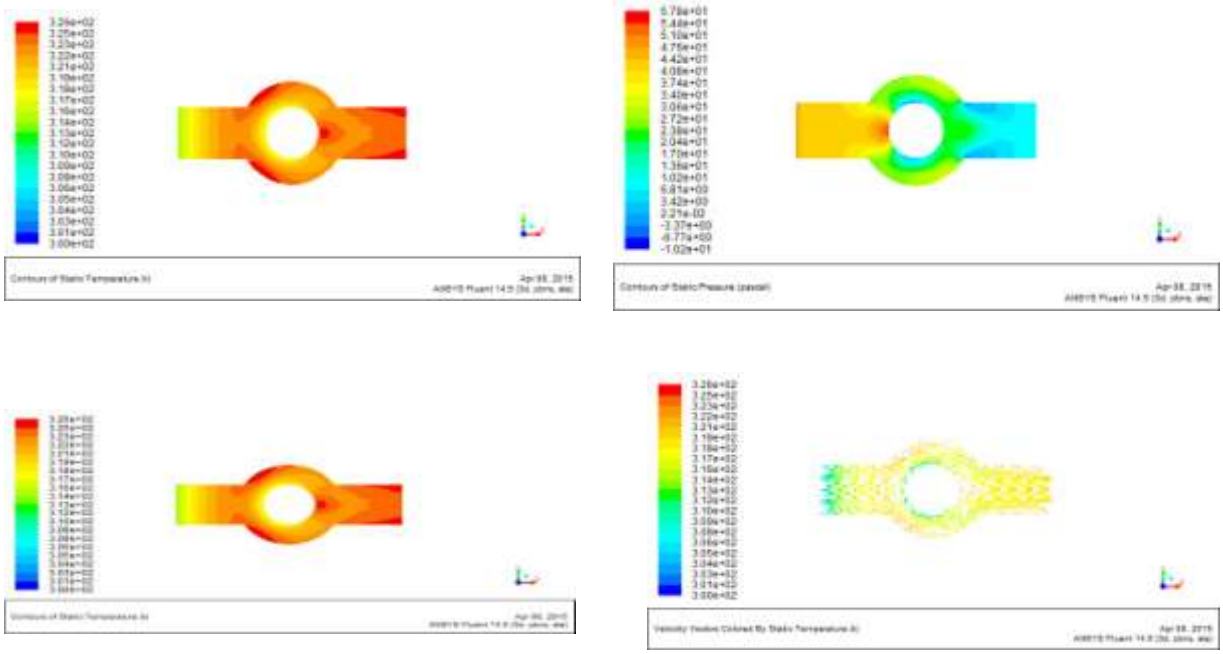

Fig: 31 Configuration 4 contour plots

Configuration 4 is similar to 2nd configuration but the only difference is that there is no copper plate covering the obstacle. The results obtained are very similar to 2nd configuration but the temperature raise is slightly lesser .These results are as shown in figure 31 for configuration 4.

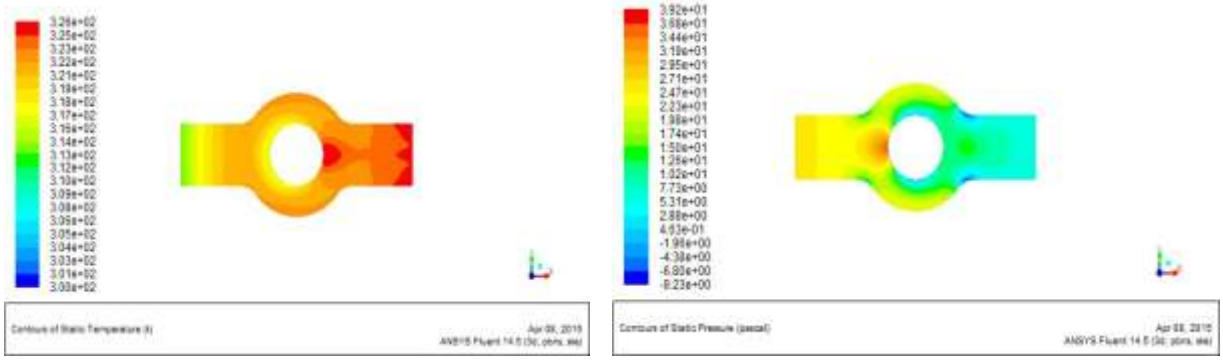

For Configuration 5 a fillet is given in the 4th configuration which has led to an increase in the Nusselt number whereas a decrease in temperature raise .The pressure drop has decreased too. These results are as shown in figure 32 for configuration 5.

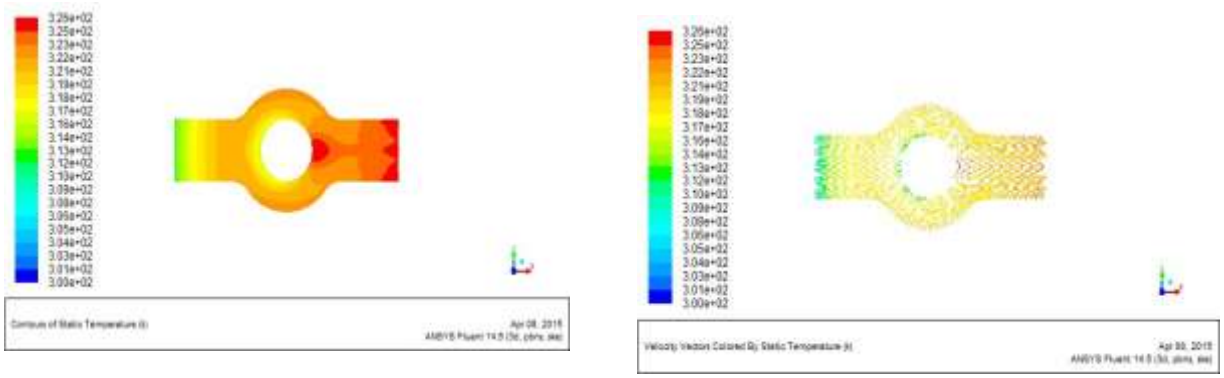

Fig: 32 Configuration 5 contour plots

B. TABULATION OF RESULTS

A. Simulation results

The results obtained can be tabulated as follows-

Table II:Analysis and conclusion

No.	Description	Temperature Coefficient	Absorber Plate Temperature Coefficient	Nusselt Number	Pressure Drop
1	Plain Model	0.0229233	0.0838	71.731	15.407
2	Without fillet with obstacle	0.0288767	0.0838	77.04	36.22
3	With fillet with obstacle	0.0255100	0.0813	80.3	20.522
4	Without fillet without plate	0.0255100	0.0741	77.147	35.94
5	With fillet without plate	0.0224033	0.0716	80.486	20.4872

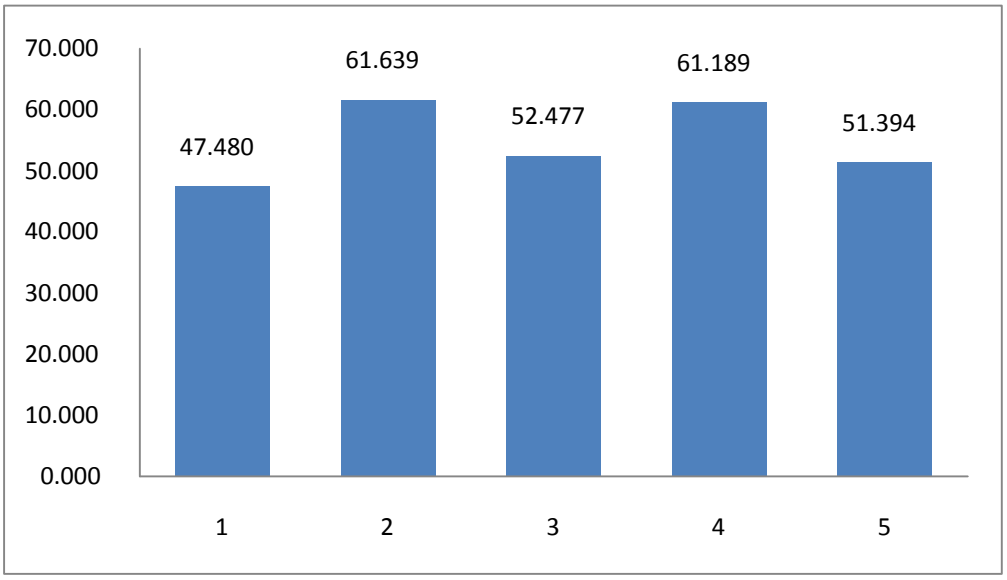

Fig: 33Temperature variation

The tables II, figures 33, 34 and 35 show the analysis and conclusion table, temperature variation , pressure variation and Nusselt numberplotrespectively which give the values of various parameters like temperature coefficient, absorber plate temperature coefficient, nusselt number and pressure drop for each of the configurations for comparative study.

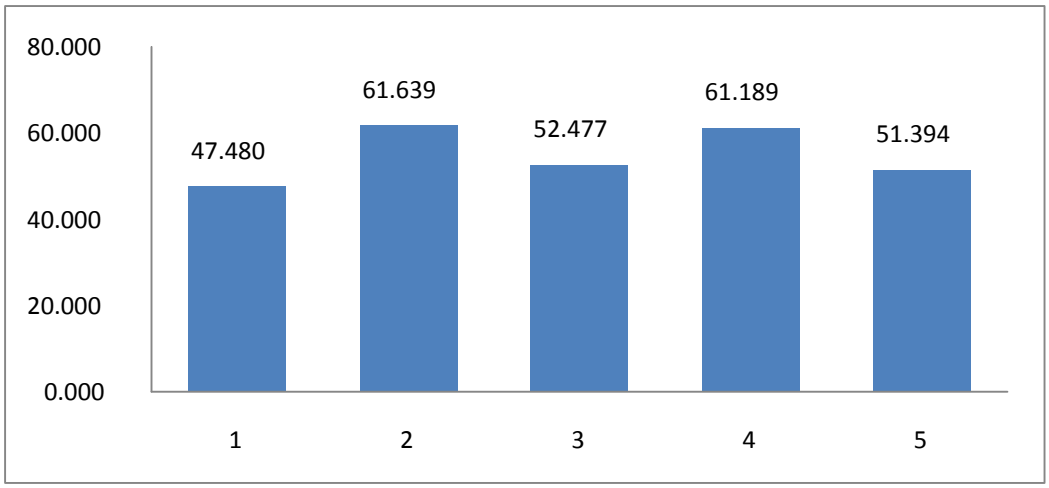

Fig: 34Pressure variation

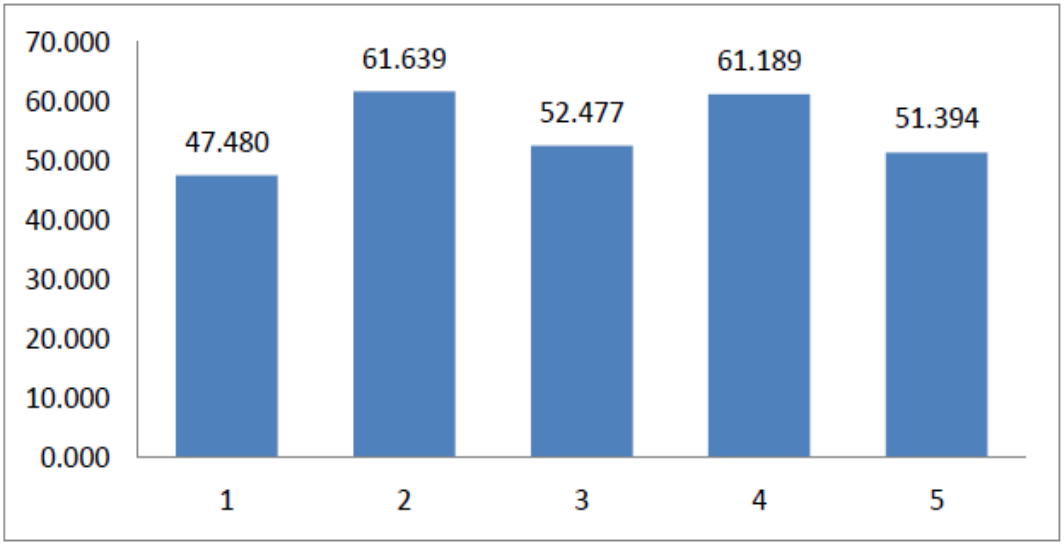

Fig: 35Nusselt number plot

B. Experimental results

The experimental results are shown in table V and VI are used for comparison with numerical results for appropriate validation.

Table V:Experimental results 1

		Reading 1		Reading 2		Reading 3		Reading 4		Reading 5	
		Model 1	Model 2	Model 1	Model 2	Model 1	Model 2	Model 1	Model 2	Model 1	Model 2
Average Velocity		2.567	3.133	2.65	2.47	2.95	3.28	2.48	2.78	2.90	2.43
Heat Flux		800.000	805.000	792.50	825.00	742.50	740.00	667.50	665.50	730.00	702.50
Inlet Air Temperature		35.000	37.000	37.00	36.00	38.00	37.50	39.00	38.00	35.00	35.00
Outlet Air Temperaure		40.733	44.800	43.83	43.90	44.47	44.60	43.90	43.60	42.10	42.95
Temperature Difference		5.733	6.950	6.83	7.90	6.47	7.10	4.90	5.60	7.10	7.95
Absorber Plate Temperature	Inlet	46.875	49.525	49.13	49.10	48.88	47.85	45.78	46.28	45.15	47.89
	Outlet	53.300	52.625	57.20	53.03	56.05	52.85	51.90	49.38	51.93	50.48
	Center		56.325		56.70		54.10		52.79		54.29
Difference between model1 and model 2		1.217		1.07		0.633		0.70		0.850	

Table V:Experimental results 2

		Reading 5		Reading 6		Reading 7		Reading 8		Reading 9	
		Model 1	Model 2	Model 1	Model 2	Model 1	Model 2	Model 1	Model 2	Model 1	Model 2
Average Velocity		2.90	2.43	3.23	3.02	2.53	3.13	2.38	2.68	2.55	2.33
Heat Flux		730.00	702.50	780.00	770.00	785.00	805.00	765.00	775.00	720.00	731.00
Inlet Air Temperature		35.00	35.00	37.00	37.50	38.00	37.00	37.50	37.50	38.50	38.00
Outlet Air Temperaure		42.10	42.95	43.40	44.80	44.63	44.80	43.30	44.25	43.53	44.15
Temperature Difference		7.10	7.95	6.40	7.30	6.63	7.80	5.80	6.75	5.03	6.15
Absorber Plate Temperature	Inlet	45.15	47.89	48.18	49.00	48.50	49.53	49.88	47.73	45.68	46.95
	Outlet	51.93	50.48	56.45	52.30	53.80	52.63	55.88	50.28	51.53	50.33
	Center		54.29		55.34		56.33		54.81		52.40
Difference between model1 and model 2		0.850		0.90		1.167		0.95		1.117	

VI. CONCLUSIONS

The numerical study has helped in understanding the flow phenomena and the heat transfer mechanism of the air heater and the following conclusions were drawn:

The geometrical modifications done in the flow path of the air heater with obstacles has helped in increasing the convective heat transfer coefficient with an increase in Nusselt no and air temperature, however the pressure drop has also increased to a greater extent.

For configuration 2 with obstacle without fillet the Nusselt no increases by 7% with respect to base model and air temp coefficient has increased by 25.97% with respect to base model.

For configuration 3 with fillet introduced in the geometry has shown marginal improvement in the Nusselt no by 12.73% and air temp coefficient by 11% compared to configuration 1 (plane model).

For configuration 4 with obstacle without absorber plate, it is observed that Nusselt no is higher than that of configuration 2

For configuration 5 with obstacle without absorber plate and with fillet, it is observed that Nusselt number is the highest compared to all other configuration and however temperature coefficient rise is marginally lower than that of configuration 3

The filleting provided in the geometry of flow path of air heater has contributed in reducing the pressure drop and increase in temp of air

The absorber plate provided for the obstacle does not contribute to the convective heat transfer capability of the air.

The experimental results were in accordance with the numerical results as shown in table V and VI

The second model with copper obstacle showed a higher outlet air temperature rise of about 1 degree centigrade as compared to the first model.

The experiment was carried out over a range of heat fluxes and the 2nd configuration always showed better results. Hence it proves that the introduction of copper obstacle improved the thermal efficiency.

ACKNOWLEDGEMENTS

I wish to express my deep sense of gratitude toDr. K Vasudeva Karanth, Professor, Department of Mechanical and Manufacturing Engineering, for guiding me with valuable support and worthy suggestions as well as encouragement throughout the course of the work. The computational facilities were provided by the Department of Mechanical and Manufacturing Engineering, Manipal Institute of Technology, Manipal, India which is appreciatively acknowledged.

REFERENCES

[1]. Gao, W., Lin, W., and Lu, E., 2000, Numerical study on natural convection inside the channel between the flat plate cover and sine-wave absorber of a cross-corrugated solar air heater. Energy Conversion and Management, 41, 145-151.

[2]. Gao, W., Lin, W., Liu, T. and Xia, C., 2007, Analytical and experimental studies on the thermal performance of cross-corrugated and flat-plate solar air heaters. Applied Energy, 84, 425-441.

[3]. Villar, N.M., et al., 2009, Numerical 3D simulations on flat plate collectors.Solar Energy,83, 1086-1092.

[4]. Wang, C., Guan, Z., Zhao, X., and Wang, D., 2006, Numerical Simulation Study on Transpired Solar Air Collector, Renewable Energy Resources and a Greener Future, 8, 3-4.

[5]. Gertzos, K.P. &Caouris, Y.G., 2007, Experimental and computational study of the developed flow field in a flat plate integrated collector storage (ICS) solar device with recirculation. Experimental Thermal and Fluid Science, 31, 1133-1145.
[6]. Gama, R.M.S., 1986, Analysis of a v-groove solar collector with a selective glass cover. Solar Energy, 36, 509–519.
[7]. Gorla, R.S.R., 1997. Finite element analysis of a flat plate solar collector. Finite Elements in Analysis and Design, 24, 283-290.
[8]. Karim, A.&Hawlader, M.N.A., 2004. Performance investigation of flat plate, v- corrugated and finned air collectors. Energy, 31, 452-470.
[9]. Turgut, O.&Onur, N., 2009.Three dimensional numerical and experimental study of forced convection heat transfer on solar collector surface. International Communications in Heat and Mass Transfer, 36(3), 274-279.
[10]. ANSYS Fluent 14.5 User's manual, Ansys Inc. (2013)